Clusters of the hydronium ion (H3O+) with H2, N2 and CO molecules

ARTICLE *in* CHEMICAL PHYSICS LETTERS · JUNE 2006

Impact Factor: 1.9 · DOI: 10.1016/j.cplett.2006.04.065

5 AUTHORS, INCLUDING:

Yehia M Ibrahim
Pacific Northwest National Laboratory
72 PUBLICATIONS **643** CITATIONS
SEE PROFILE

Enli Xie
Virginia Commonwealth University
4 PUBLICATIONS **43** CITATIONS
SEE PROFILE

Michael Noah Mautner
Virginia Commonwealth University
202 PUBLICATIONS **5,206** CITATIONS
SEE PROFILE

M. Samy El-Shall
Virginia Commonwealth University
272 PUBLICATIONS **4,604** CITATIONS
SEE PROFILE

Available online at www.sciencedirect.com
SCIENCE DIRECT
Chemical Physics Letters 424 (2006) 257–263
CHEMICAL PHYSICS LETTERS
www.elsevier.com/locate/cplett

Clusters of the hydronium ion (H_3O^+) with H_2, N_2 and CO molecules

Ridha Mabourki, Yehia Ibrahim, Enli Xie, Michael Meot-Ner (Mautner), M. Samy El-Shall *

Department of Chemistry, Virginia Commonwealth University, Richmond, VA 23284-2006, United States

Received 7 March 2006; in final form 13 April 2006
Available online 27 April 2006

Abstract

The thermochemistry of $H_3O^+(X)_n$ clusters (X = H_2, N_2 and CO and n = 1–3) was determined by equilibrium measurements using the mass selected drift tube technique. The binding energies for $H_3O^+(H_2)_n$ (n = 1 and 2) are 3.4 and 3.5 kcal mol^{-1}, and for $H_3O^+(N_2)_n$ (n = 1–3) are 7.8, 7.3 and 6.3 kcal/mol, respectively. The binding energy of the polar CO molecule is 11.2 kcal mol^{-1}, and ab initio calculations show that the $H_2OH^+\cdots CO$ conformation is more stable than the $H_2OH^+\cdots OC$ conformation. Saddle point energy of 17.6 kcal/mol is calculated for inversion between these conformational isomers.

1. Introduction

The hydronium ion plays central roles in aqueous solutions, where it interacts with solutes, including dissolved gases. Such interactions also occur in ionized planetary atmospheres and in interstellar clouds where H_3O^+ ions can interact with major gas components such as hydrogen, nitrogen and carbon monoxide [1]. The gas phase clustering of these molecules around the hydronium ion is of fundamental interest and is relevant to important processes. Specifically, the thermochemistry of the bonding of H_3O^+ to small gaseous molecules is needed to model the relevant atmospheric and astrophysical interactions. However, few data are available on the bonding energies of H_3O^+ to common gases [2]. The reported cluster binding energies vary from small for H_2 to substantial for the polar SO_2 molecule, with reported bond dissociation enthalpies (kcal mol^{-1}) of; H_2, 3.5 [3]; CO_2, 14.3–15.3, 20.7 [4–6], N_2O, 16.9 [7], and SO_2, 22.0 [6].

One reason for the scarcity of data is that equilibrium methods such as high pressure mass spectrometry require H_2O to be present in the reaction system to generate H_3O^+ ions. However, in such a mixture the strongly bonded $H_3O^+(H_2O)_n$ clusters predominate and prevent equilibrium with more weakly bonded ligands. An ideal experiment would allow the injection and thermalization of H_3O^+ ions into a dry gas such as X (where X = H_2, N_2 or CO) held at a controlled temperature and pressure. In addition, the approach to equilibrium between the $H_3O^+(X)_{n-1}$ and $H_3O^+(X)_n$ ions must be directly established.

In the present work, we use a mass-selected drift cell technique to measure the thermochemistry of the clusters of H_3O^+ with several molecules of H_2, N_2 and CO. We also present ab initio structures and energies of these clusters. In the clustering of H_3O^+ with the CO molecule, it is of interest whether the adduct is a covalent $(HCOOH)H^+$ ion or a non-covalent cluster, and if a cluster, whether it is bonded by $H_2OH^+\cdots CO$ or $H_2OH^+\cdots OC$ bonds. We shall present experimental and theoretical evidence to answer these questions.

2. Experimental and computational methods

The experiments were performed using the VCU mass-selected ion mobility tandem mass spectrometer. The details of the instrument can be found in several publications [8,9], and only a brief description of the experimental procedure is given here. Mass-selected H_3O^+ ions (produced by electron impact ionization of water clusters generated by a pulsed supersonic beam expansion of 1% water vapor in 3000 Torr He) are injected (in 5–15 μs

* Corresponding author. Fax: +1 804 828 1280.
E-mail address: selshall@hsc.vcu.edu (M. Samy El-Shall).

0009-2614/$ - see front matter © 2006 Elsevier B.V. All rights reserved.
doi:10.1016/j.cplett.2006.04.065

pulses) into the drift cell containing 0.2–1.0 Torr of pure H_2, N_2 or CO vapor. The drift cell has dimensions of 8.1 cm inner diameter and 8.9 cm length. Flow controllers (MKS #1479A) are used to maintain a constant pressure inside the drift cell. The temperature of the drift cell can be controlled to better than ±1 K using six temperature controllers. Liquid nitrogen flowing through solenoid valves is used to cool down the drift cell. The reaction products can be identified by scanning a second quadrupole mass filter located coaxially after the drift cell. The arrival time distributions (ATD) are collected by monitoring the intensity of each ion as a function of time. The reaction time can be varied by varying the drift voltage. The injection energies used in the experiments (5–20 eV, laboratory frame) are slightly above the minimum energies required to introduce the ions into the cell against the gas flow. Most of the ion thermalization occurs outside the cell entrance by collisions with the vapor escaping from the cell entrance orifice [8,9]. At a cell pressure of 0.2 Torr, the number of collisions that the H_3O^+ encounters from the neutral molecules within the 1.5 ms residence time inside the cell is about 10^4 collisions, which is sufficient to ensure efficient thermalization of the H_3O^+ ions. The ATDs of the injected H_3O^+ and the $(H_3O^+)(X)_n$ formed inside the cell are measured as a function of the drift voltage across the cell. The ion intensity ratio $(H_3O^+)(X)_n/(H_3O^+)(X)_{n-1}$ is measured from the integrated peak areas of the ATDs as a function of decreasing cell drift field corresponding to increasing reaction time, and equilibrium is achieved when a constant ratio is obtained. Equilibrium constants are then calculated from $K = [I(H_3O^+\cdot X_n)/I(H_3O^+\cdot X_{n-1})P(A)]$ where I is the integrated ion intensity taken from the ATD and P(A) is the partial pressure of the neutral A in the drift cell. A good test of equilibrium is the observation of identical ATDs of the reactant and product ions. If the $H_3O^+\cdot X_n$ and $H_3O^+\cdot X_{n-1}$ ions are in equilibrium, their ATDs must be identical. All the equilibrium experiments at different temperatures are conducted at correspondingly low drift fields and long residence times (1.35 ms). The measured equilibrium constant is independent of the applied field across the drift cell in the low field region. The equilibrium constant measured as a function of temperature yields $\Delta H°$ and $\Delta S°$ from the van't Hoff equation [$\ln K = -\Delta H°/RT + \Delta S°/R$]. All the results were reproduced at least three times.

Ab initio calculations at four different levels of theory were carried out with the GAUSSIAN03 software [10].The calculated binding energies reported here were corrected for the unscaled-ZPE and BSSE (basis set superposition error). The BSSE was calculated utilizing the Counterpoise method as implemented in GAUSSIAN03.

3. Results and discussion

Figs. 1-A and 1-B display typical examples of the mass spectra and arrival time distributions of the $(H_3O^+)(H_2)_n$ and $(H_3O^+)(N_2)_n$ clusters. As shown in Fig. 1-A, at a temperature of −104 °C only the H_3O^+ is observed. However, as the temperature decreases to −146 °C $(H_3O^+)(H_2)_n$ with $n = 1$ and 2 are clearly observed. Similarly, the mass spectra in Fig. 1-B indicate that at −110 °C, the $(H_3O^+)(N_2)_n$

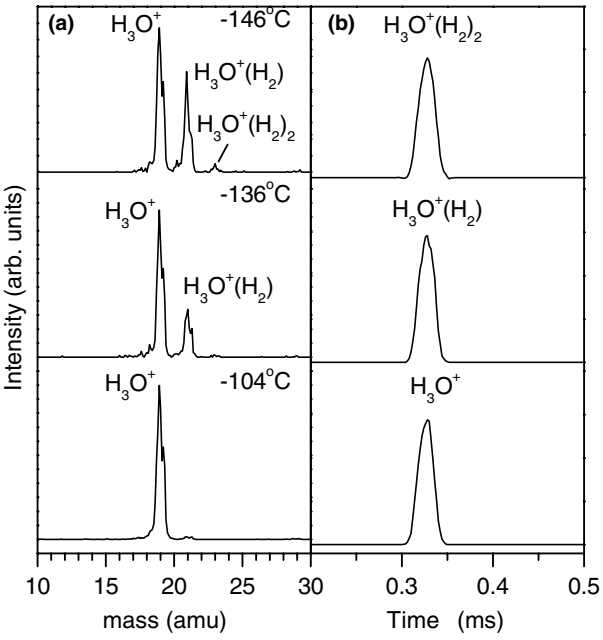

Fig. 1-A. (a) Mass spectra obtained following the injection of H_3O^+ (*m/z* 19) into a drift cell containing 0.5 Torr of pure H_2 at different temperatures. (b) Arrival time distributions (ATDs) of $H_3O^+(H_2)_n$ with $n = 0$–2 measured at −146 °C.

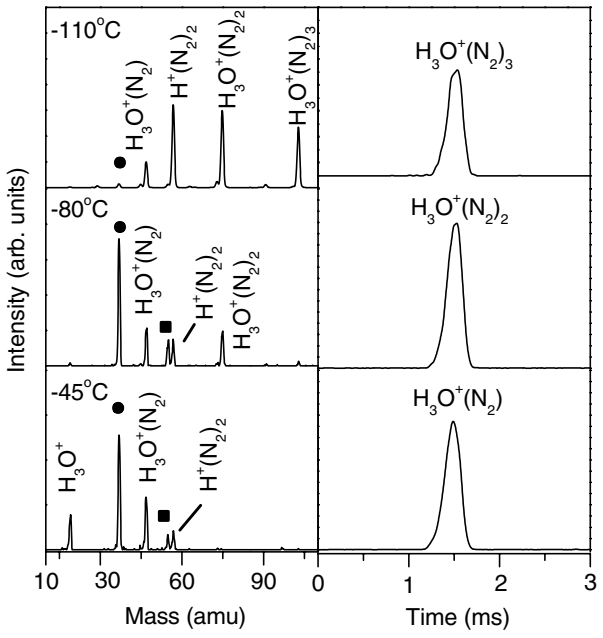

Fig. 1-B. (a) (left) Mass spectra obtained following the injection of H_3O^+ (*m/z* 19) into a drift cell containing 0.5 Torr of pure N_2 at different temperatures. Protonated water dimers (H^+W_2, *m/z* 37) and trimers (H^+W_3, *m/z* 55) are observed due to the presence of a trace amount of water vapor in the drift cell. Protonated nitrogen dimers ($H^+(N_2)_2$, *m/z* 57) are also observed. (right) Arrival time distributions (ATDs) of $H_3O^+(N_2)_n$ with $n = 1$–3 measured at −110 °C.

clusters with $n = 1$–3 are the major ions observed. Other significant ions present include $H^+(N_2)_2$ at −110 °C and $(H_3O^+)(H_2O)_n$ with $n = 1$–2 in the temperature range −45 to −80 °C. The $(H_3O^+)(H_2O)_n$ are formed due to the presence of impurity water vapor in the N_2 gas. However, at lower temperatures the water vapor freezes and the protonated water clusters essentially disappear. The ATDs shown in Figs. 1-A(b) and 1-B (right) clearly indicate that ions in each of the $(H_3O^+)(H_2)_n$ and $(H_3O^+)(N_2)_n$ clusters groups are coupled by association equilibria. The equilibrium constants for the stepwise clustering of H_2, N_2 and CO on H_3O^+ yielded the van't Hoff plots shown in Fig. 2. The resulting $\Delta H°$ and $\Delta S°$ values, along with the calculated ab initio binding energies are listed in Tables 1 and 2. Figs. 3, 4 and 5-A display the ab initio geometries and atomic charges of the calculated lowest energy clusters.

The effect of the level of theory on the calculated binding energies of the H_2 molecules to H_3O^+ is clearly evident from the results shown in Table 1. It appears that a higher level of electron correlation, as in the B3LYP/6-311++G** calcula-

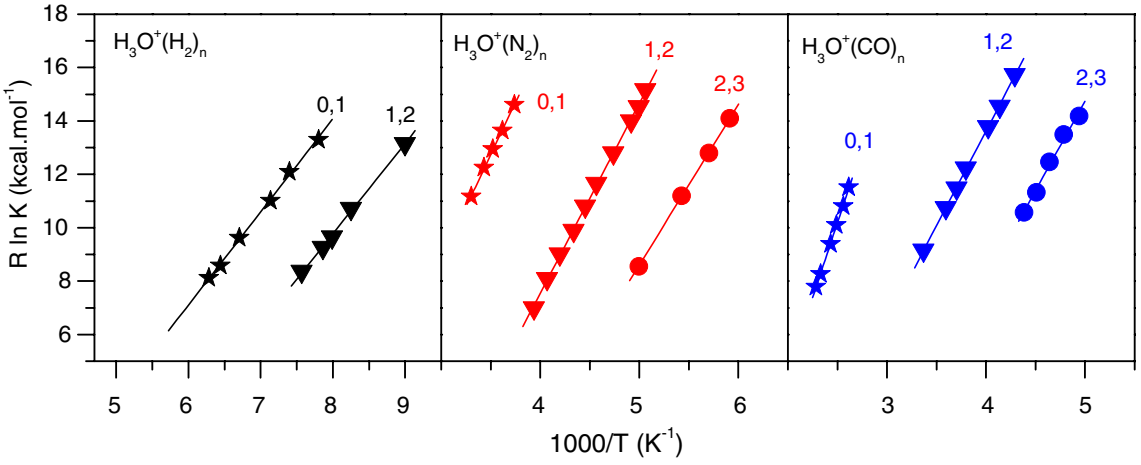

Fig. 2. Van't Hoff plots for the equilibria $H_3O^+(X)_{n-1} + X = H_3O^+(X)_n$ for X = H_2, N_2 and CO and for $n - 1$, n as shown.

Table 1
Calculated binding energies of $H_3O^+(X)_{n-1} + H_2 = H_3O^+(X)_n$ for X = H_2 and N_2 at various levels, and experimental thermochemistry of the clustering reactions[a]

n	MP2//ROHF/6-31+G**	MP2/6-31+G**	MP2/6-311++G**	B3LYP/6-311++G**	$\Delta H°_{n-1,n}$ (exp)	$\Delta S°_{n-1,n}$ (exp)
Ligand = H_2						
1	−1.0	−0.8	−1.9	−3.5	−3.4	−13.8
2	−0.9	−0.7	−1.7	−3.0	−3.5	−17.3
3	−0.9	−0.8	−1.65	−2.6		
Ligand = N_2						
1	−7.6	−7.8	−8.4	−9.6	−7.9	−14.8
2	−6.5	−6.6	−7.1	−7.7	−6.9	−20.0
3	−6.0	−6.0	−6.4	−6.6	−5.4	−17.6
4	−2.6					

[a] Binding energies and $\Delta H°$ in (kcal mol^{-1}), $\Delta S°$ in (cal mol^{-1} K^{-1}). Estimated uncertainty $\Delta H°$ ± 1 kcal mol^{-1}, $\Delta S°$ ± 2 cal mol^{-1} K^{-1}.

Table 2
Calculated binding energies of $H_3O^+(CO)_{n-1} + CO = H_3O^+(CO)_n$ at various levels of theory[a]

N		MP2//ROHF/6-31+G**	MP2/6-31+G**	MP2/6-311++G**	B3LYP/6-311++G**	$\Delta H°_{n-1,n}$ (exp)	$\Delta S°_{n-1,n}$ (exp)
1	CO	−11.8	−13.3	−14.0	−14.7	−11.5	−18.6
	OC	−6.4	−5.8	−5.3	−8.2		
2	CO	−9.4	−9.9	−10.2	−10.2	−9.8	−23.8
	OC	−5.6	−5.2	−4.8	−6.8		
3	CO	−8.1	−8.5	−8.8	−8.5	−8.6	−27.4
	OC	−5.2	−4.8	−4.5	−6.1		
4	CO	−2.3					

'CO' denotes the $H_3O^+(CO)_n$ and 'OC' denotes the $H_3O^+(OC)_n$ conformations.
[a] Binding energies and $\Delta H°$ in (kcal mol^{-1}), $\Delta S°$ in (cal mol^{-1} K^{-1}). Estimated uncertainty $\Delta H°$ ± 1 kcal mol^{-1}, $\Delta S°$ ± 2 cal mol^{-1} K^{-1}.

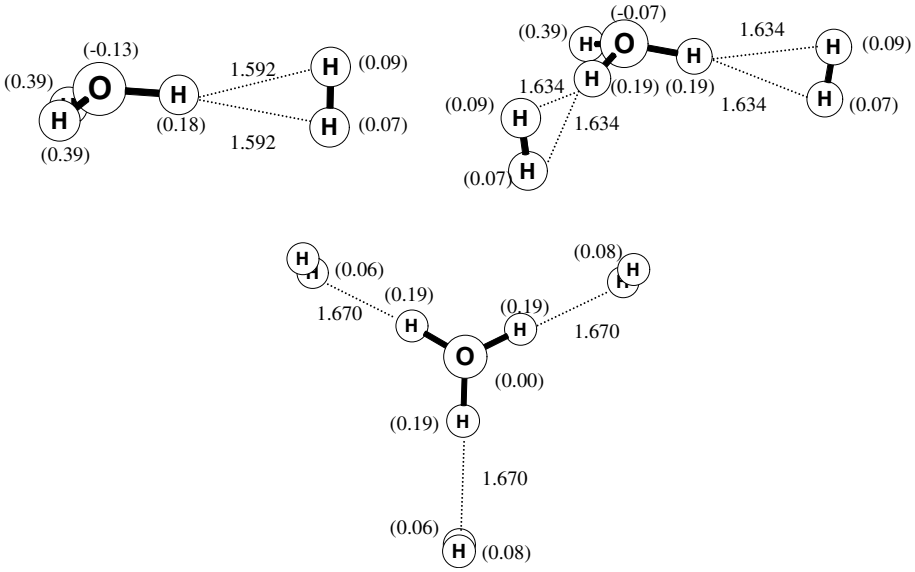

Fig. 3. Optimized structures of $H_3O^+(H_2)_{1-3}$ at B3LYP/6-311++G** level. Bond lengths are in Angstrom and atomic charges are in parenthesis.

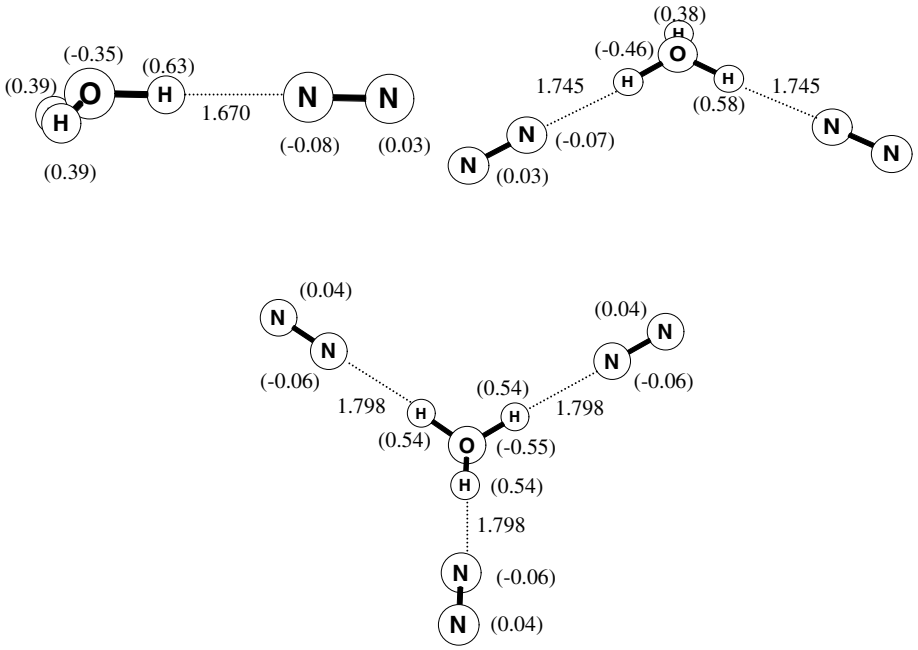

Fig. 4. Optimized structures of $H_3O^+(N_2)_{1-3}$ at B3LYP/6-311++G** level. Bond lengths are in Angstrom and atomic charges are in parenthesis.

tion, may be required to capture most of the details of the interactions between weakly binding hydrogen molecules and the H_3O^+ ion. As for the N_2 and CO molecules, the B3LYP/6-311++G** calculation appears to overestimate the binding energies of the first ligand to the H_3O^+ ion.

The experimental bonding energies show a small decrease in the stepwise bonding energies in each set. With the weakly bonding H_2 the first two binding energies are equal. With the more strongly bonding N_2 and CO, the consecutive ligands have larger mutual effects. However, the effects of all of these ligands on the core ion are small. For example, the remaining unbounded hydrogens retain a charge of 0.39–0.37 when none to two molecules of any of these ligands, respectively are attached to the core ion. The ligand molecules show some mutual steric interference, as the entropy change for adding the second ligand molecule is larger than the first one in all of the three sets.

An interesting result of the calculations is that $H_2OH^+\cdots CO$ is more strongly bonded than the $H_2OH^+\cdots OC$ isomer, although in the latter the negative part of the ligand's dipole is closer to the proton charge. This is consistent with the much higher proton affinity of CO at the carbon atom, 142 kcal mol^{-1} vs. at the oxygen atom, 102 kcal mol^{-1} [11]. The stronger bonding in $H_2OH^+\cdots CO$ suggests covalent contributions to the -$H^+\cdots CO$ bond. Similar effects were observed in hydrogen

bonded complexes of isocyanides vs. cyanides with protonated amines, $R_3NH^+\cdots CNR$ vs. $R_3NH^+\cdots NCR$. Both of these clusters and the present $H_2OH^+\cdots CO$ complexes involve sp carbon lone pairs that facilitate covalent contributions to the hydrogen bond [12].

To address the binding of CO with H_3O^+ in more detail, a potential-energy surface scan was generated by varying the C···H bond length (in 0.05 Å step size) and the OCH angle (in 1° step size) and calculating the energy at each step. The starting and final geometries were those for the optimized $H_2OH^+\cdots CO$ and $H_2OH^+\cdots OC$ structures at the B3LYP/6-311++G** level. The energy for the final product differed from that obtained by geometry optimization of $H_2OH^+\cdots OC$ at B3LYP/6-311++G** by 1.6 kcal/mol. This difference comes from the small difference in the OCHO dihedral angle between the two structures. The resulting potential energy surface, shown in Fig. 5-B, predicts a saddle point energy of 17.6 kcal/mol for the inversion of $H_2OH^+\cdots CO$ to the $H_2OH^+\cdots OC$ isomer.

Another interesting aspect of this system is that $H_2OH^+\cdots CO$ is a non-covalent isomer of the covalent $(HCOOH)H^+$ protonated formic acid. Using tabulated thermochemical data [11], the energy of covalent association of $H_3O^+ + CO$ to give this product would be −18.4 kcal/mol, more exothermic than the observed association energy of −11.5 kcal/mol. Evidently the observed adduct is the non-covalent complex. Also, the entropy of covalent association is usually −40 to −60 cal mol^{-1} K^{-1}, vs. the −18.6 cal mol^{-1} K^{-1} measured for the $H_3O^+ +$ CO association.

The comparative thermochemistry of covalent vs. non-covalent adducts was investigated [13,14] and reviewed recently [15]. In the present case, the thermochemistry indicates non-covalent association. The complex could be converted to the covalent adduct through proton shift to carbon and a cyclic intermediate such as:

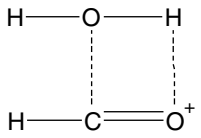

The transition from the complex to the adduct is exothermic but probably has a high barrier. This system is of interest for interstellar chemistry, since CO and H_2O are major interstellar molecules in these protonating environments, and their neutral adduct HCOOH product is also observed. If field-driven energetic collisions can overcome the barrier, this ionic mechanism could form interstellar

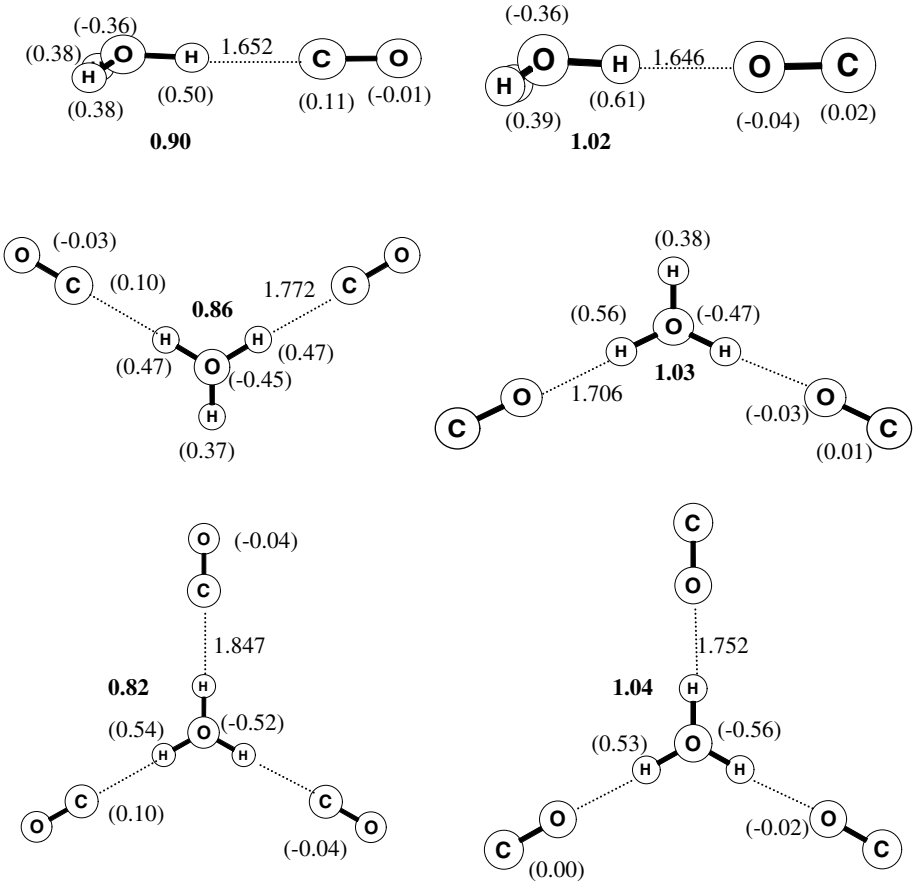

Fig. 5-A. Optimized structures of $H_3O^+(CO)_{1-3}$ and $H_3O^+(OC)_{1-3}$ and at B3LYP/6-311++G** level. Bond lengths are in Angstrom while the molecular charges are in bold and atomic charges are in parenthesis.

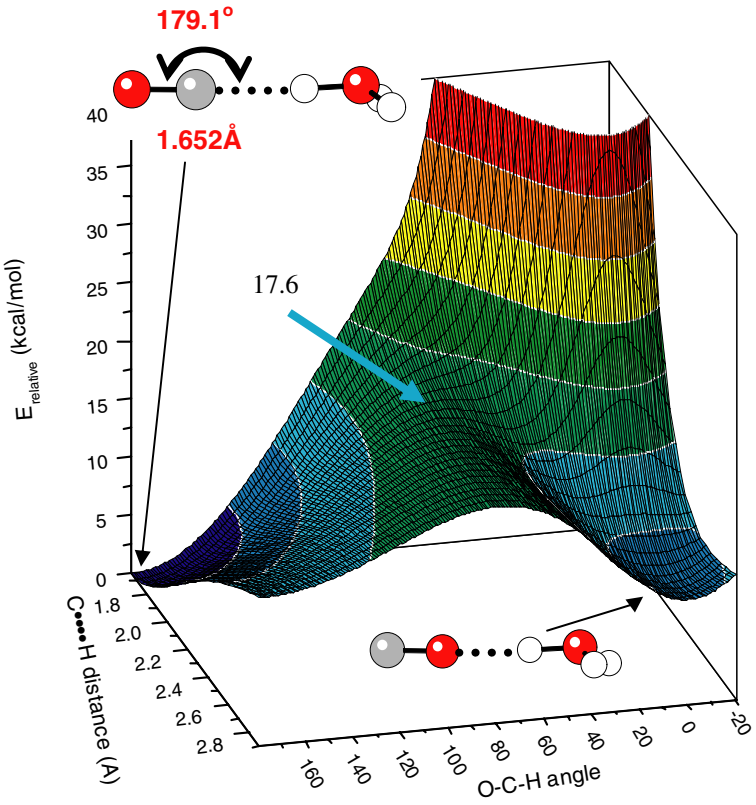

Fig. 5-B. Potential-energy surface scan for inverting the orientation of the CO molecule in the complex with H_3O^+ between the H_3O^+(CO) and H_3O^+(OC) geometries. A saddle point of 17.6 kcal/mol is indicated. The scan was obtained at the B3LYP/6-311++G** level of theory.

formic acid. The other complexes of H_3O^+ investigated here are also important in interstellar clouds and planetary atmospheres subject to protonating conditions since H_2O, H_2, N_2 and CO are all significant components in these environments [1]. Since cluster formation through termolecular processes is not very likely in the low-density astrochemical environments, these complexes can be stabilized by non-collisional mechanisms involving fast radiative stabilization particularly in large complexes with many vibrational degrees of freedom.

4. Summary

The association energies of H_3O^+ with several H_2, N_2 and CO molecules were measured. The bonding energies for the addition of 1–3 ligand molecules vary little in each set, as all of ligand molecules can bind directly to the protons of the H_3O^+ ion in the first solvation shell, as shown by the ab initio calculations. The CO molecules form $H_2OH^+\cdots CO$ bonded clusters where the carbon lone pair can contribute a covalent component, consistent with other systems involving hydrogen bonds of carbon lone pairs. This conformation is also consistent with the higher proton affinity of CO on carbon vs. oxygen. Although the bond strengths in the present clusters are small, they can be stable in low temperature planetary ionospheres and in interstellar clouds.

Acknowledgement

This work was funded by National Science Foundation (CHE-0414613) and NASA (NNG04GH45G) Grants to VCU (M.S.E.).

References

[1] E. Herbst, Ann. Rev. Phys. Chem. 46 (1995) 27.
[2] M. Meot-Ner (Mautner), S.G. Lias, The Thermochemistry of Cluster Ions, in: P.J. Linstrom, W.G. Mallard (Eds.), NIST Chemistry WebBook, NIST Standard Reference Database Number 69, National Institute of Standards and Technology, Gaithersburg MD, 2005. Available from: <http://webbook.nist.gov> .
[3] M. Okomura, L.I. Yeh, J.D. Myers, Y.T. Lee, J. Phys. Chem. 94 (1990) 3416.
[4] M. Meot-Ner (Mautner), F.H. Field, J. Chem. Phys. 66 (1977) 4527.
[5] K. Hiraoka, T. Shoda, K. Morise, S. Yamabe, E. Kawai, K. Hirao, J. Chem. Phys. 84 (1986) 2091.
[6] J. Szulejko, T.B. McMahon, T.B. Unpublished values cited in Ref. [1].
[7] K. Hiraoka, S. Fujimaki, K. Aruga, T. Sato, S. Yamabe, J. Chem. Phys. 101 (1994) 4073.
[8] M.J. Rusyniak, Y. Ibrahim, E. Alsharaeh, M. Meot-Ner (Mautenr), M.S. El-Shall, J. Phys. Chem. A 107 (2003) 7656.
[9] M.J. Rusyniak, Y. Ibrahim, D.L. Wright, S.N. Khanna, M.S. El-Shall, J. Am. Chem. Soc. 125 (2003) 12001.
[10] M.J. Frisch et al., GAUSSIAN 03, Revision C.02, Gaussian, Inc., Wallingford CT, 2004.
[11] E.P. Hunter, S.G. Lias, Proton Affinity Evaluation, in: P.J. Linstrom, W.G. Mallard (Eds.), NIST Chemistry WebBook, NIST Standard

Reference Database Number 69, National Institute of Standards and Technology, Gaithersburg MD. Available from: <http://webbook.nist.gov> .
[12] M. Meot-Ner (Mautner), L.W. Sieck, K.K. Koretke, C.A. Deakyne, J. Am. Chem. Soc. 119 (1997) 10430.
[13] M. Meot-Ner (Mautner), M.M. Ross, J.E. Campagna, J. Am. Chem. Soc. 107 (1985) 4839.
[14] K. Norrmann, T.B. McMahon, J. Am. Chem. Soc. 118 (1996) 2449.
[15] M. Meot-Ner (Mautner), Chem. Rev. 105 (2005) 213.